Selective layer disordering in intersubband $Al_{0.028}Ga_{0.972}N$/AlN superlattices with silicon nitride capping layer

2015 Appl. Phys. Express 8 061004

(http://iopscience.iop.org/1882-0786/8/6/061004)

Applied Physics Express **8**, 061004 (2015)
http://dx.doi.org/**10.7567/APEX.8.061004**

Selective layer disordering in intersubband $Al_{0.028}Ga_{0.972}N$/AlN superlattices with silicon nitride capping layer

Jonathan J. Wierer, Jr.*, Andrew A. Allerman, Erik J. Skogen, Anna Tauke-Pedretti, Gregory A. Vawter, and Ines Montaño

Sandia National Laboratories, Albuquerque, NM 87185, U.S.A.
E-mail: jwierer@sandia.gov

Received March 7, 2015; accepted May 10, 2015; published online June 1, 2015

Selective layer disordering in an intersubband $Al_{0.028}Ga_{0.972}N$/AlN superlattice using a silicon nitride (SiN_x) capping layer is demonstrated. The SiN_x capped superlattice exhibits suppressed layer disordering under high-temperature annealing. Additionally, the rate of layer disordering is reduced with increased SiN_x thickness. The layer disordering is caused by Si diffusion, and the SiN_x layer inhibits vacancy formation at the crystal surface and ultimately, the movement of Al and Ga atoms across the heterointerfaces. Patterning of the SiN_x layer results in selective layer disordering, an attractive method to integrate active and passive III–nitride-based intersubband devices.

AlGaN-based heterostructures have large conduction band offsets to support intersubband transitions at telecommunication wavelengths (1.3 and 1.55 μm).[1–4] Various III–nitride intersubband devices have been demonstrated, such as optical modulators,[5,6] quantum cascade lasers,[7] and photodetectors.[8,9] However, these demonstrations are limited to discrete devices, and there is an absence of processing methods to integrate multiple devices to create photonic integrated circuits, as has been done in other III–V compound semiconductors. For III–nitride intersubband devices to compete with existing technologies, new integration techniques are required.

One powerful method employed in conventional III–V compound semiconductors for device integration is layer disordering (or intermixing).[10,11] In this method, the diffusion of vacancies and/or impurities within the semiconductor lattice causes movement (or rearrangement) of the crystal lattice atoms. In heterostructures, this rearrangement of lattice atoms, and in particular the column III atoms, causes heterointerfaces to become less abrupt. If structures such as quantum wells (QWs) are layer disordered, the electronic states within the QWs shift in energy. For interband (bandgap) transitions, this results in a blue shift in wavelength, and, in intersubband transitions, it results in a red shift in wavelength. If this method is selective (area site specific), one can produce portions of the superlattice that are not absorbing.[11–13] These non-absorbing areas can be transformed into passive elements such as low-loss waveguides to route photons between active optical devices.

Layer disordering is also possible in III–nitride semiconductors. It has been demonstrated in highly Si-doped QWs used for intersubband absorption when subject to high growth temperatures or post-growth high temperature annealing.[14] At high temperatures, Si diffuses out of the QWs and into the barriers of the superlattice, which promotes layer disordering of the heterointerfaces. Reference 14 shows that the conduction energy band diagram of the intermixed QWs has less abrupt heterointerfaces and a "rounded" shape. The first and second electron states become closer in energy, causing a red shift in the absorption wavelength. In addition, the first electron state is elevated in energy, resulting in a reduced electron population and a decrease in the amount of absorption. Layer disordering is prevented (mitigated) at growth temperatures lower than 885 °C and is a fundamental material property regardless of the method used to grow the III–nitride heterostructure. Layer disordering with the as-grown doping is not selective, or site-specific, though, and necessitates an alternative method to make this possible. Most recently, it has been shown that ion implantation can affect absorption in III–nitride-based intersubband structures and can also be used to modify the absorption selectively.[15]

In this letter, a silicon nitride (SiN_x) cap layer is shown to inhibit layer disordering of the heterointerfaces in Si-doped AlGaN/AlN intersubband structures. Layer disordering occurs at a slower rate in the portions of the superlattice capped with SiN_x compared to the uncapped portions. Additionally, as the thickness of the SiN_x layer increases, the rate of layer disordering decreases. These data suggest that the SiN_x layer prevents vacancy formation at the crystal surface, inhibiting Si diffusion and layer disordering. This letter presents a method to use the doping present in the sample to promote selective layer disordering of the structure.

The intersubband superlattice structures used in this study are grown by metal–organic vapor phase epitaxy (MOVPE) on (0001) sapphire substrates misoriented by 0.2° toward the *m*-plane. First, ~2-μm-thick AlN template layers with dislocation densities (DDs) of $\sim 3 \times 10^9\,cm^{-2}$ and $\sim 10^{10}\,cm^{-2}$ are grown. Next, a superlattice is grown, at 800 °C, consisting of 20 periods of $Al_{0.028}Ga_{0.972}N$ QWs and AlN barrier layers that are ~14.5 and ~45 Å thick, respectively. The $Al_{0.028}Ga_{0.972}N$ QWs are Si-doped with an electron concentration of $\sim 7 \times 10^{19}\,cm^{-3}$. The superlattice has an intersubband absorption centered near ~1.56 μm. The structure is capped with a ~20-nm-thick AlN layer. All data presented correspond to superlattices grown on a low DD, except where the rate of layer disordering is compared versus DD.

After growth, the intersubband samples are formed into waveguides by cutting out ~8–10-mm-long pieces and polishing 45° facets to create a multipass waveguide. This waveguide is used to measure the intersubband absorption in a Fourier transform infrared spectrometer with a near-infrared polarizer to measure only transverse magnetic (TM) light. This measurement is performed on as-grown and annealed samples with and without SiN_x capping layers.

Following growth, portions of the samples are deposited with SiN_x using plasma-enhanced chemical vapor deposition (PECVD) using silane and nitrogen as sources at a temperature of 250 °C. SiN_x with thicknesses of 50, 150, 200, and 250 nm are deposited in order to determine the layer disordering rate with thickness. After deposition, the absorp-

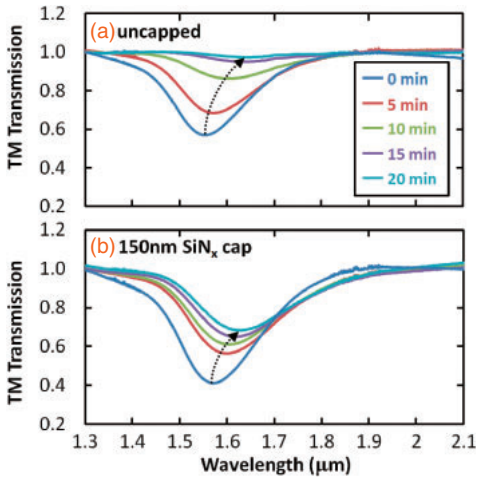

Fig. 1. TM transmission versus wavelength for an (a) uncapped and a (b) 150-nm-thick SiN_x-capped $Al_{0.028}Ga_{0.972}N/AlN$ superlattice. The layer disordering is suppressed in the capped portion of the sample.

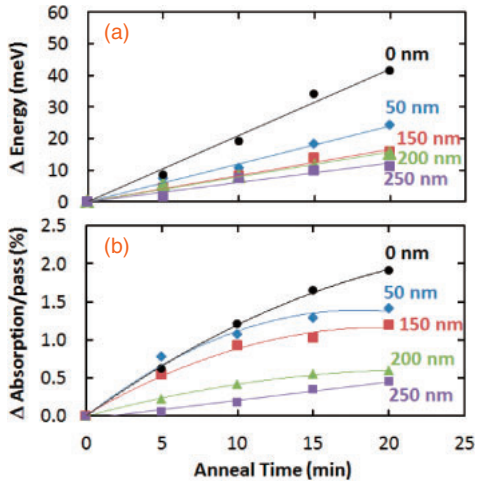

Fig. 2. Change in (a) energy and (b) absorption per pass versus annealing time of $Al_{0.028}Ga_{0.972}N/AlN$ superlattices with SiN_x cap thicknesses of 0, 50, 150, 200, and 250 nm. As the thickness of the SiN layer increases, the changes in energy and absorption decrease.

tion spectra of the samples are measured without annealing. Then the samples are placed epitaxial side up in a rapid thermal annealer (RTA) and subject to 5 min anneals at 1000 °C in N_2. The annealing occurred for multiples of 5 min intervals for a cumulative total of 20 min, and absorption measurements are performed after each interval.

Simulations to determine the Al–Ga interdiffusion coefficient ($D_{Al–Ga}$) of the Si-doped $Al_{0.028}Ga_{0.972}N/AlN$ superlattices are performed using an intersubband absorption simulator. The simulation takes into account a) the impact of spontaneous and piezoelectric polarization[16,17] and the screening potential introduced by charged carriers on the band structure and b) the impact of many-body effects[18–20] on the absorption spectrum using a density-matrix approach.[21] The band structure parameters are given in Ref. 22. This set of parameters is chosen to match the experimental trends for interband transitions in AlGaN semiconductors and consists of parameters from several publications.[23–25]

The transmission versus annealing time for the sample with a 150-nm-thick SiN_x layer is compared to the uncapped portion of the same sample in Fig. 1. With increased annealing time, both the uncapped and capped portions exhibit a red shift in wavelength and a decrease in absorption strength. The SiN_x-capped areas redshift and decrease in absorption at a much slower rate compared to the uncapped portions. Clearly, the SiN_x affects the rate of layer disordering. Since the layer disordering is determined by the diffusion of Si doping within the QWs,[14] the SiN_x changes the rate of Si diffusion within the sample.

To explore this further, the thickness of the SiN_x layer was varied using similar samples. The resulting change in peak absorption energy and absorption per pass are plotted in Fig. 2. The uncapped data (SiN_x thickness of 0 nm) is an average of all the uncapped areas of the samples. All samples exhibit a change in energy and decrease in absorption, but, as the thickness of the SiN_x layer increases, the change in energy and absorption decreases. This dependence of layer disordering on the thickness of the SiN_x layer is another indication that the SiN_x has an effect on the Si diffusion within the samples. The use of a capping layer to modify

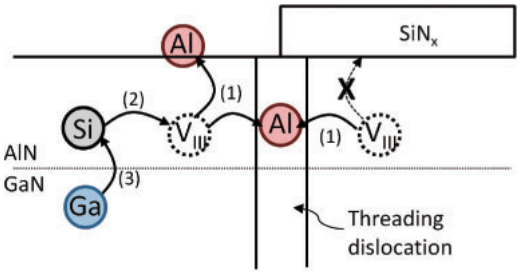

Fig. 3. Cross-sectional schematic of an AlN/GaN heterostructure with and without a SiN_x capping layer to illustrate the layer disordering progression. Existing column-III vacancies (V_{III}) or those created by the surface and threading dislocations (1) present a site into which Si can move (2). This in turn promotes the movement of other column-III lattice atoms (3) and the interlayer disordering of the heterointerfaces. The SiN_x layer prevents this additional vacancy formation and reduces the rate of layer disordering.

layer disordering has been observed in other semiconductor material systems,[26–28] but it has not been demonstrated in III–nitride semiconductors before.

The dependence of layer disordering on the presence and thickness of the SiN_x layer suggests the following layer disordering mechanism. A schematic representation of this mechanism is shown in Fig. 3. Si is necessary for layer disordering, as demonstrated previously.[14] Vacancies, such as column III vacancies (V_{III}), are more easily created at the uncapped sample surfaces compared to SiN_x capped surfaces through the 20 nm AlN capping layer. The Si diffuses along one path with a substitutional mechanism via V_{III}. The movement of the Si allows for the Al or Ga to backfill the V_{III} sites, promoting intermixing of Al-rich and Ga-rich AlGaN QWs and barrier layers. The SiN_x suppresses V_{III} formation and hence layer disordering. Furthermore, as the SiN_x thickness increases, the air interface becomes farther from the superlattice surface, and, in turn, V_{III} formation and layer disordering are further suppressed.

The SiN_x layer cannot completely prevent layer disordering, indicating that there is a finite amount of vacancies in the as-grown superlattice and other possible sources for vacancy creation. This could be an explanation for differences in layer disordering that are found with different growth methods.[29,30]

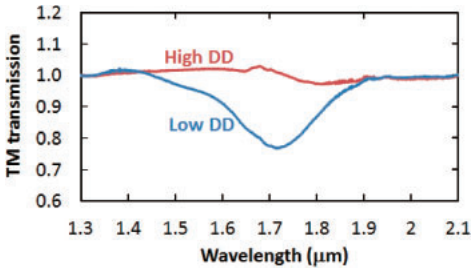

Fig. 4. TM transmission versus wavelength for an $Al_{0.028}Ga_{0.972}N/AlN$ superlattice grown on a high-dislocation-density (DD) and low-DD AlN template layer. The high-DD superlattice has a smaller absorption that is red-shifted from the superlattice on the low-DD template layer, showing that dislocations can provide an additional vacancy formation path within the superlattice.

Other possibilities are the crystallinity of the SiN_x and its propensity to prevent (or promote) vacancies within the III–nitride structure and the thickness of the AlN capping layer. These topics require further research.

Yet another possible source of vacancies is threading dislocations, which are prevalent in III–nitride semiconductors grown on sapphire substrates. Therefore, a change in the number of threading dislocations should affect the rate of layer disordering. To test this hypothesis, superlattices are grown on AlN template layers with different DDs (low DD $\sim 3 \times 10^9\,cm^{-2}$ and high DD $\sim 10^{10}\,cm^{-2}$). The transmission of these two samples is shown in Fig. 4. The absorption in the higher-dislocation-density sample is much less than in the low-dislocation-density sample. Additionally, the absorption of the high-DD sample is red-shifted ($\sim 1.8\,\mu m$) from the absorption of the low-DD sample, consistent with the post-growth annealing data shown above. The threading dislocations within the superlattice provide a large amount of surface area for additional vacancy formation and subsequent layer disordering. In this case, the layer disordering occurs during growth, but these dislocations are also available for vacancy formation in post-growth annealing and should contribute to the layer disordering show in Figs. 1–3.

Another possible explanation for the differences in absorption of the two dislocation samples is the differences in interface roughness. To discount this hypothesis, atomic force microscopy images of the surface are considered representative of what is occurring at the heterointerfaces within the superlattice. It was found that higher-dislocation-density samples tend to have lower root-mean-square roughness than low-dislocation-density samples. Therefore, if layer disordering were not occurring, one would expect the high-dislocation sample to have sharper interfaces and be blue-shifted from the low-dislocation samples. The opposite is observed in Fig. 4, further confirming that layer disordering is stronger in samples with higher DDs.

These data suggest that threading dislocations can be an additional source for vacancy formation even if a SiN_x cap layer is used. It is expected that the SiN_x capping of intersubband samples to prevent layer disordering will become more effective as the threading DD is reduced. This can be accomplished by using, for example, low-dislocation bulk substrates such as AlN and GaN.

Figure 5 shows simulation and experimental data to determine the dependence of the Al–Ga interdiffusion

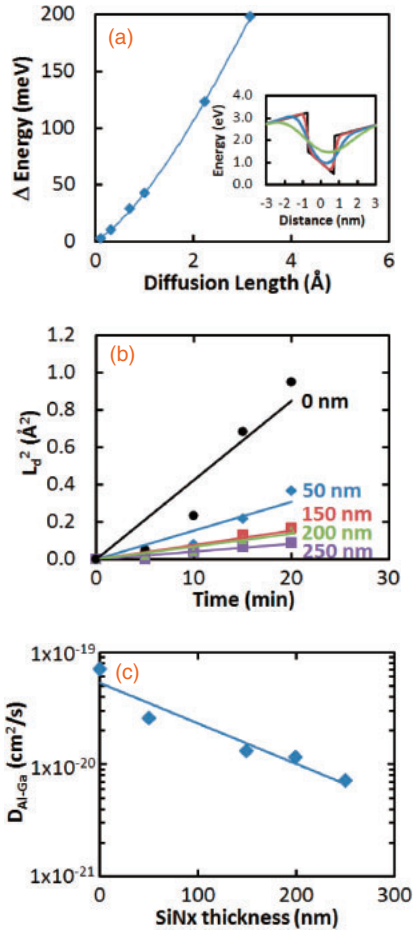

Fig. 5. Simulation results of (a) the change in energy versus diffusion length using the energy band diagram in the inset. Plot of (b) diffusion length squared versus time for superlattices with different thicknesses of SiN_x capping layers. Plot of (c) the Al–Ga interdiffusion coefficient versus thickness of the SiN_x capping layer.

coefficient (D_{Al-Ga}) on the thickness of the SiN_x capping layer in the low-dislocation superlattices. During layer disordering, the heterointerfaces become less abrupt [inset of Fig. 5(a)], and the electronic states within the QWs shift in energy. The composition of the layer disordered QWs are modeled with an error function, where the Al composition Al(x) is given by:[31]

$$\mathrm{Al}(x) = \mathrm{Al}_{\mathrm{bar}}\left[1 + \frac{1}{2}\,\mathrm{erf}\left(\frac{x - L_x/2}{2L_d}\right) - \frac{1}{2}\,\mathrm{erf}\left(\frac{x + L_x/2}{2L_d}\right)\right], \quad (1)$$

where Al_{bar} is the initial Al composition in the barrier, L_x is the QW thickness, L_d is the diffusion length, and x is the growth direction of the superlattice. The diffusion length (L_d) is defined as:

$$L_d = \sqrt{D_{Al-Ga}t}, \quad (2)$$

where t is the diffusion time. Inputting the results of Eq. (1) into the intersubband absorption simulator provides the change in absorption peak energy versus diffusion length, as shown in Fig. 5(a). This plot provides L_d as a function of the change in intersubband energy (ΔEnergy) and is fitted with a third-order polynomial. Using this function along with the change in energy versus annealing time in Fig. 2(a), the diffusion length squared versus time is determined, and is

shown in Fig. 5(b). A close look at Fig. 5(b) shows that the fit to the bare samples is far from perfect, while the capped samples have a much better fit. This may be because the intersubband absorption is nearly depleted at longer annealing times (Fig. 1), and determination of the exact transition energy becomes more difficult. Finally, Fig. 5(c) shows the $D_{\mathrm{Al–Ga}}$ versus SiN_x thickness using the linear fits from Fig. 5(b). As the SiN_x thickness increases, the $D_{\mathrm{Al–Ga}}$ decreases. The coefficient changes by two orders of magnitude, showing that SiN_x has a profound impact on the layer disordering in the superlattice. The $D_{\mathrm{Al–Ga}}$ is much lower than that of other III–V semiconductors, such as AlGaAs,[26,32] due to the higher bonding strengths in III–nitrides. It is also lower than the interdiffusion coefficients for InGaN/GaN structures.[33]

In summary, this selective layer disordering technique can be used in III–nitride semiconductors in ways similar to those used in other III–V compound semiconductors. In this study, the superlattice is doped during growth, which is typically done to fabricate absorptive intersubband devices such as modulators. Using this selective disordering technique, one can integrate active modulators with passive elements, such as low-loss waveguides. Of course, other challenges remain to create efficient waveguides in III–nitride intersubband structures. For example, scattering losses due to surface or interface roughness need to be mitigated. This could be achieved by growing on native bulk substrates such as AlN or GaN, which may present smoother surfaces and result in smoother interfaces. The selective disordering technique, however, is potentially a useful processing tool to enable photonic integrated circuits in III–nitride intersubband structures.

Acknowledgments The authors would like to thank F. Cajas for the waveguide preparation. This work is fund by the Sandia National Laboratories Laboratory Directed Research and Development program. Sandia National Laboratories is a multi-program laboratory managed and operated by Sandia Corporation, a wholly owned subsidiary of Lockheed Martin Corporation, for the U.S. Department of Energy's National Nuclear Security Administration under contract DE-AC04-94AL85000.

1) C. Gmachl, H. M. Ng, S. N. G. Chu, and A. Y. Cho, Appl. Phys. Lett. **77**, 3722 (2000).
2) N. Suzuki and N. Iizuka, Jpn. J. Appl. Phys. **38**, L363 (1999).
3) D. Hofstetter, E. Baumann, F. R. Giorgetta, R. Theron, H. Wu, W. J. Schaff, J. Dawlaty, P. A. George, L. F. Eastman, F. Rana, P. K. Kandaswamy, F. Guillot, and E. Monroy, Proc. IEEE **98**, 1234 (2010).
4) M. Beeler, E. Trichas, and E. Monroy, Semicond. Sci. Technol. **28**, 074022 (2013).
5) N. Suzuki and N. Iizuka, Jpn. J. Appl. Phys. **36**, L1006 (1997).
6) N. Iizuka, K. Kaneko, and N. Suzuki, Electron. Lett. **40**, 962 (2004).
7) G. Sun, R. A. Soref, and J. B. Khurgin, Superlattices Microstruct. **37**, 107 (2005).
8) D. Hofstetter, S. S. Schad, H. Wu, W. J. Schaff, and L. F. Eastman, Appl. Phys. Lett. **83**, 572 (2003).
9) D. Hofstetter, E. Baumann, F. R. Giorgetta, R. Théron, H. Wu, W. J. Schaff, J. Dawlaty, P. A. George, L. F. Eastman, F. Rana, P. K. Kandaswamy, S. Leconte, and E. Monroy, J. Phys.: Condens. Matter **21**, 174208 (2009).
10) W. D. Laidig, N. Holonyak, Jr., M. D. Camras, K. Hess, J. J. Coleman, P. D. Dapkus, and J. Bardeen, Appl. Phys. Lett. **38**, 776 (1981).
11) D. Hofstetter, B. Maisenholder, and H. P. Zappe, IEEE J. Sel. Top. Quantum Electron. **4**, 794 (1998).
12) K. Meehan, J. M. Brown, P. Gavrilovic, N. Holonyak, R. D. Burnham, T. L. Paoli, and W. Streifer, J. Appl. Phys. **55**, 2672 (1984).
13) R. L. Thornton, D. F. Welch, R. D. Burnham, T. L. Paoli, and P. S. Cross, Appl. Phys. Lett. **49**, 1572 (1986).
14) J. J. Wierer, Jr., A. A. Allerman, and Q. Li, Appl. Phys. Lett. **97**, 051907 (2010).
15) J. J. Wierer, Jr., A. A. Allerman, E. J. Skogen, A. Tauke-Pedretti, C. Alford, G. A. Vawter, and I. Montaño, Appl. Phys. Lett. **105**, 131107 (2014).
16) S. L. Chuang, IEEE J. Quantum Electron. **32**, 1791 (1996).
17) S. L. Chuang and C. S. Chang, Phys. Rev. B **54**, 2491 (1996).
18) J. Förstner, K. J. Ahn, J. Danckwerts, M. Schaarschmidt, I. Waldmüller, C. Weber, and A. Knorr, Phys. Status Solidi B **234**, 155 (2002).
19) Y. S. Kim, A. Kaneta, M. Funato, Y. Kawakami, T. Kyono, M. Ueno, and T. Nakamura, Appl. Phys. Express **4**, 052103 (2011).
20) X. Li, X. Ni, J. Lee, M. Wu, U. Ozgur, H. Morkoc, T. Paskova, G. Mulholland, and K. R. Evans, Appl. Phys. Lett. **95**, 121107 (2009).
21) K. A. Bulashevich, O. V. Khokhlev, I. Y. Evstratov, and S. Y. Karpov, Proc. SPIE **8278**, 827819 (2012).
22) J. J. Wierer, Jr., I. Montano, M. Crawford, and A. A. Allerman, J. Appl. Phys. **115**, 174501 (2014).
23) I. Vurgaftman and J. R. Meyer, in *Nitride Semiconductor Devices: Principles and Simulations*, ed. J. Piprek (Wiley, New York, 2007) p. 169.
24) I. Vurgaftman, J. R. Meyer, and L. R. Ram-Mohan, J. Appl. Phys. **89**, 5815 (2001).
25) W. Bardyszewski and S. P. Lepkowski, Phys. Rev. B **85**, 035318 (2012).
26) J. S. Major, F. A. Kish, T. A. Richard, A. R. Sugg, J. E. Baker, and N. Holonyak, J. Appl. Phys. **68**, 6199 (1990).
27) L. J. Guido, J. S. Major, J. E. Baker, W. E. Plano, N. Holonyak, K. C. Hsieh, and R. D. Burnham, J. Appl. Phys. **67**, 6813 (1990).
28) W. J. Choi, S. M. Han, S. I. Shah, S. G. Choi, D. H. Woo, S. Lee, S. H. Kim, J. I. Lee, K. N. Kang, and J. Cho, IEEE J. Sel. Top. Quantum Electron. **4**, 624 (1998).
29) D. Hofstetter, J. Di Francesco, D. Martin, N. Grandjean, Y. Kotsar, and E. Monroy, Appl. Phys. Lett. **98**, 241101 (2011).
30) J. S. Yang, H. Sodabanlu, M. Sugiyama, Y. Nakano, and Y. Shimogaki, Appl. Phys. Lett. **95**, 162111 (2009).
31) J. D. Ralston, S. Obrien, G. W. Wicks, and L. F. Eastman, Appl. Phys. Lett. **52**, 1511 (1988).
32) K. J. Beernink, R. L. Thornton, G. B. Anderson, and M. A. Emanuel, Appl. Phys. Lett. **66**, 2522 (1995).
33) C. C. Chuo, C. M. Lee, and J. I. Chyi, Appl. Phys. Lett. **78**, 314 (2001).